LIQUID FILM CHARACTERIZATION IN HORIZONTAL ANNULAR FLOW USING OPTICAL TECHNIQUE

P.S.C. Farias, paula.farias@puc-rio.br
F.J.W.A. Martins, fabio.jessen@gmail.com
Department of Mechanical Engineering, PUC-Rio, Rio de Janeiro, Brazil
L.E.B. Sampaio, luizebs@vm.uff.br
Department of Mechanical Engineering - Laboratory of Theoretical and Applied Mechanics - LMTA/PGMEC, UFF, Rio de Janeiro, Brazil
L.F.A. Azevedo, Lfaa@puc-rio.br
Department of Mechanical Engineering, PUC-Rio, Rio de Janeiro, Brazil

Abstract. *A non-intrusive optical technique was employed to provide time-resolved images of the liquid film of horizontal annular flow of air and water, revealing the interfacial wave behavior. Time-resolved images of the pipe cross section revealed the dynamics of the complete liquid film around the pipe wall. The planar laser induced fluorescence technique (PLIF) was implemented to allow for the optical separation of the light emitted by the film from that (more intense) scattered by the air-water interface. The visualization test section was fabricated from a tube material which has nearly the same refractive index as water, what allowed for the visualization of the liquid film at regions very close to the pipe wall. Longitudinal images of the liquid film were captured using a high speed digital video camera synchronized with a high repetition rate laser. Data sets were collected with sampling camera frequencies ranging from 250 to 3000 Hz. A specially developed image processing algorithm was employed to automatically detect the position of the air-water interface in each image frame. The thickness of the liquid film was measured in each processed image frame, providing time history records of the film thickness in whole image. Wave velocities were measured by cross-correlating the amplitude signals from two axial positions of the thickness data. Wave frequency information was obtained by analyzing the time-dependent signals of film thickness recorded. The results obtained allowed for the verification of the variation of the liquid film characteristics with global flow parameters, such as the liquid and gas flow superficial velocities. For the film cross section observations, two high speed digital video cameras were used in a stereoscopic arrangement. The high repetition rate laser had its laser sheet mounted so as to illuminate a pipe cross section. Images from the left and right cameras were dewarped by the use of a calibration target and an image correction algorithm. Dewarped images from each camera were then joined to yield the complete instantaneous cross section image of the liquid film. Comparisons with results from different techniques available in literature indicate that the present technique shows equivalent accuracy in measuring the liquid film properties. The stereoscopic technique developed is an original contribution of the present work to the set of experimental techniques available for the study of two-phase flows. Time–resolved images of longitudinal and cross section views of the film were recorded and analyzed, what constitutes in valuable information for the understanding of the dynamics of the liquid film in horizontal annular flow.*

Keywords*: optical film characterization, annular flow, time-resolved laser induced fluorescence*

1. INTRODUCTION

Annular two-phase flow regime is important for the operation of several industrial equipments such as refrigeration systems, nuclear reactors and steam boiler. In horizontal annular regime gas flows in the pipe core, while the liquid flows as a thin non-uniform film around the tube wall. The gas phase usually contains liquid droplets entrained from the liquid film surface and the liquid phase includes two types of wave configuration. The first one is small ripples on the base film that move at low velocities and do not appear to carry mass. The second structure, disturbance waves, carries mass along the tube and travels at a higher velocity. The mechanisms that maintain the film at the upper pipe wall, compensating drainage induced by gravity, have not been fully resolved yet. Possible physical mechanisms of liquid transport that have been proposed over the years can be summarized in the works of Butterworth and Pulling (1972) and Jayanti *et al.* (1990). These mechanisms are (i) secondary gas motion induced by the circumferentially varying film thickness, (ii) liquid entrainment and re-deposition, (iii) wave spreading due to the distortion of liquid film waves at the bottom of the tube and (iv) pumping action associated with the flow of gas over the disturbance waves. Recently, Oliveira and Portela (2010) proposed another mechanism based on the axial gradient of the shear stress at the film interface.

For many years measurements of the wave structure of the liquid film have been conducted for vertical and horizontal annular flows. Resistance probes (Jayanti *et al.*, 1990 and Paras and Karabelas, 1991) and optical methods were employed (Shedd and Newell, 1998) to determine the local time variation of film thickness, wave velocity and frequency, as well as spectral properties of film thickness time records.

Several research groups have developed visualization techniques as a tool to aid in characterizing the film wave behavior along the years. Ciné movie with steady external illumination was used in conjunction with dye injection by

Taylor and Nedderman (1968) and by Butterworth and Pulling (1972). Later, high speed video systems were introduced and replaced the time-consuming movie processing (Hewitt et al., 1990). Sutharshan et al. (1995) employed the photochromic dye activation technique to generate fluid tracers within the liquid film that were followed by high-speed digital imaging equipment with external back lighting. The analysis of the digital images provided qualitative information on the effects of wave passage on the liquid axial and circumferential velocity in the film.

Typical liquid films in horizontal annular flow have such small dimensions at the neighborhood of a solid wall, what is a challenge for optical techniques. Hewitt et al. (1990) used an index-matched test section to minimize the distortions caused by the curvature of the tube. The tube, fabricated from fluorinated ethylene propylene (FEP), presented nearly the same index of refraction as water, what allowed for the clear visualization of the film structure close to the wall. Rodríguez and Shedd (2004) employed the same tube material in a visualization setup based on the planar laser induced technique (PLIF). In this technique a fluorescent dye dissolved in water and excited by a pulsed planar sheet of laser light is used to produce images of the air-water interface. The reflections from the interface are blocked by an optical filter placed in front of the digital camera, producing instantaneous images of longitudinal sections of the film. Attempts to measure liquid velocity within the film were made by Vassalo (1999) using hot film probes in vertical annular flow. More recently, Koplin (2004) obtained partial success with particle image velocimetry (PIV) and particle tracking techniques to estimate velocity field in the film. A novel technique was presented by Belt et al. (2010), where an array of conductive probes flush mounted around the tube inner surface provided instantaneous axial and circumferential information on the liquid film distribution.

The present work is part of an ongoing research project aimed at providing simultaneous, time-resolved qualitative and quantitative information of the liquid in horizontal annular flows employing index of refraction matching techniques associated with PLIF. Images of the film were captured with high frame rate cameras synchronized with high-repetition rate lasers and processed to enhance contrast and to extract the time dependent properties of the flow. Two different setups were utilized, one for capturing side views of the lower portion of the liquid film and a second setup for obtaining instantaneous images of the complete cross section at a particular axial position of the tube.

2. EXPERIMENTAL FACILITY

The present study employed non-intrusive optical techniques to provide time-resolved images of the liquid film in horizontal annular air-water flows. The experimental technique implemented builds on the previous works of Hewitt et al. (1990) and Rodríguez and Shedd (2004) in the sense that employs index of refraction matching techniques associated with planar laser induced fluorescence technique (PLIF). This technique allows optical separation of the light emitted by the film from that (more intense) scattered by the air-water interface. Rhodamine B at a concentration of 500 μg per liter of water was employed as the fluorescent material. The fluorescent material was excited by a sheet of green light (527-nm wavelength) emitted by a double cavity, high-repetition rate, Nd-YLF laser.

The use of the refractive index matching was employed to minimize optical distortions by reason of the mismatch between the indexes of refraction of the tube wall material and the liquid and to allow the visualization of the thin annular liquid film. For this reason, pipes fabricated from FEP, which has nearly the same refractive index as water, were employed in the test section designed (Hewitt *et al.*, 1990).

Figure 1(a) presents a schematic view of the test section utilized in the experiments for measuring the liquid film at the lower part of the tube. Water from a pump was fed to a 15-mm-diameter FEP tube. Air was supplied to the test section by a centrifugal compressor. Air and water were mixed at a tee connection located at the inlet section of the tube. Calibrated rotameters were used to measure the air and water flow rates. The air-water flow exiting the tube was directed to a centrifugal separator from where the water was returned to the pump inlet, while the air was vented out of the laboratory space. In the visualization region at a distance of 190 diameters from the inlet the tube is surrounded by a rectangular box filled with water, as shown in Fig. 1(b). This configuration minimizes optical distortions due to the pipe wall curvature.

A Pegasus dual-cavity Nd-YLF high-repetition laser provided illumination of a longitudinal section of the tube. A pair of cylindrical and spherical lenses was used to transform the circular beam into a planar light sheet with dimensions of 25 mm wide by 0.5-mm thick. The horizontal light sheet coming from the laser was deviated by a 45° mirror so that the light entered vertically through the bottom wall of the visualization box and passed through the FEP pipe, illuminating a longitudinal section of the air-water flow inside the pipe, as indicated in Fig. 1(b).

Images of the lower portion of the liquid film were captured using an IDT Motion Pro X3 camera operating from 250 to 3000 frames per second at a spatial resolution of 512 x 512 pixels. The camera was mounted orthogonally to the light sheet plane. Nikkor lenses with focal distances of 60 and 105 mm equipped with spacer rings were employed, respectively, for the film thickness and wave speed measurements. A TSI 610035 synchronizer and the Insight-3G® software were used to synchronize laser firing and image capture. A high pass optical filter with a cutoff wave length of 560 nm was installed in front of the camera lens to block the 527-nm green laser light scattered by the air-water interfaces. With the filter installed, the camera only registered the 610-nm fluorescence light emitted by the Rhodamine dissolved in the water.

Cross sectional views of the liquid film were obtained by an optical setup employing two high frame rate cameras mounted at an angle, as indicated in Fig. 2(a). In this case, the light sheet was rotated by 90° so as to illuminate a cross section of the pipe. Two IDT Motion Pro X3 cameras were mounted at an angle of 45°, imaging the pipe cross section through the two 45-degree-inclined windows provided at the visualization box that surrounded the test tube. Each camera was mounted on a support that permitted that the camera body was rotated in relation to the lens axis. This setup allowed the attainment of the Scheimpflug condition. When this condition is attained, the whole image is focused, even though the camera is viewing the pipe cross section at an angle (Raffel *et al.*, 2007).

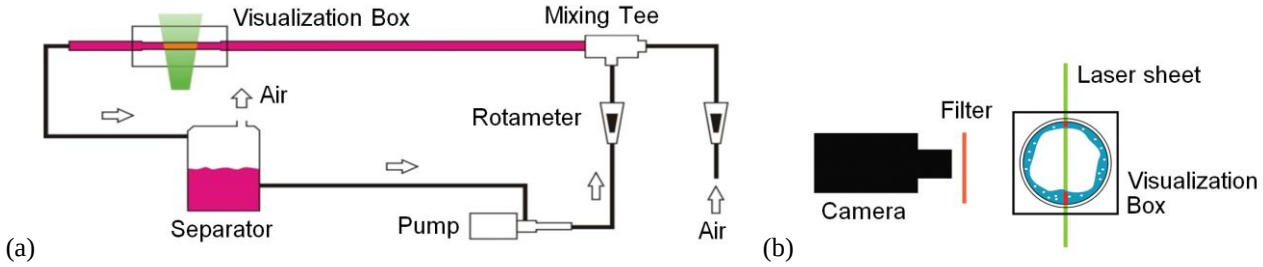

Figure 1. (a) Schematic view of the test section. (b) Optical setup for longitudinal film visualization.

The same Pegasus dual-cavity, Nd-YLF, high-repetition laser was used to provided illumination of a cross section view of the tube. Different from the longitudinal view, two light sheet laser planes were used, made by an arrangement of one beam splitter, three mirrors and two pairs of cylindrical and spherical lenses as shown in Fig. 2(b). This setup was necessary to provide a good illumination to the upper and lower portions of the liquid film inside the tube, due to the attenuation of the light sheet.

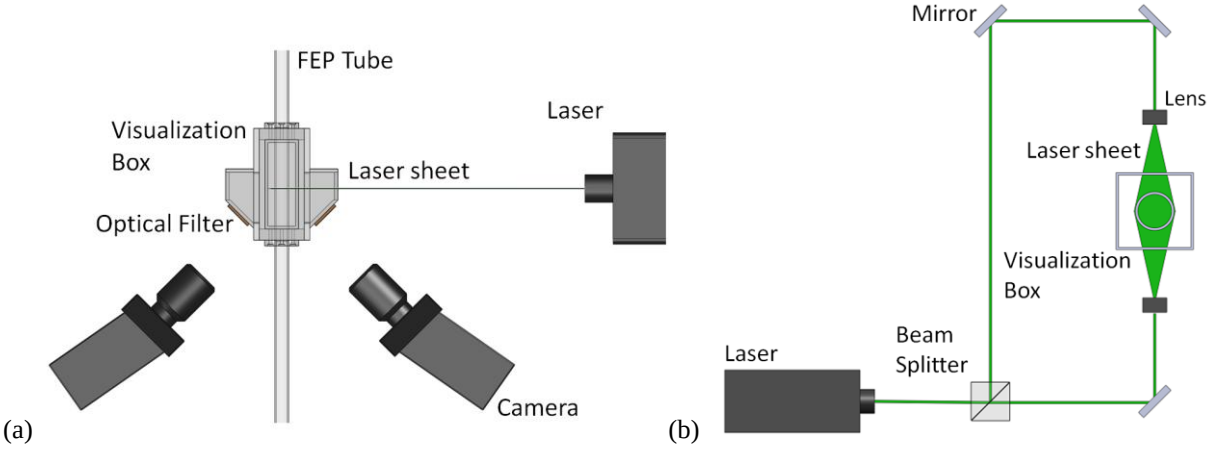

Figure 2. (a) Top and (b) transverse views of optical setup for cross section liquid film visualization.

3. IMAGE PROCESSING

The image processing procedures employed in extracting the film thickness versus time information from the set of captured images will now be outlined. All these procedures were implemented using routines available in the Matlab® software. Further details of the image processing can be found in Farias (2010).

3.1. Longitudinal images of lower liquid film

After a sequence of images of the lower liquid film for a particular combination of water and air flow rates was captured and stored, the first step in the image processing procedure is the correction of the contrast. Figure 3(a) presents a sample of a typical original instantaneous liquid film image captured by the camera. The pre-processing routine improves contrast adjusting the intensity histogram based on a sigmoid function applied in each column of the images. Figure 3(b) shows significant enhance of the contrast due to the column-based adjust over the original image. To measure the film thickness, the images are binarized as shown in Fig. 3(c). So the film thickness can be determined by counting the number of white pixels until the first black pixel is found (interface), once the position of the lower wall is input to the program. In Fig. 3(d), as a verification procedure, a white, thick line corresponding to the measured film thicknesses is overlaid on the original image, Fig. 3(a). The agreement obtained is considered excellent. The white patches over the liquid film, but not connected to it, are images of fluid out of the illumination plane, and were not computed in the film thickness measurement.

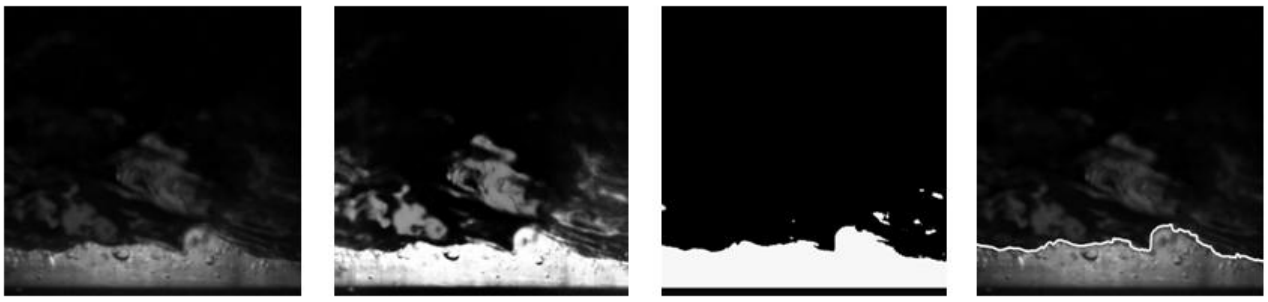

(a) (b) (c) (d)

Figure 3. (a) Original liquid film image. (b) Image after the correction of the contrast. (c) Binary image. (d) Measured liquid thickness film ovelaid on original image.

The film thickness measurements in pixels were converted to millimeters by a pixel calibration procedure. Pixel calibration of the images was obtained by using a target inserted into the test pipe through its exit section, after the removal of the return pipe connection. This target is constituted by a grid of regularly spaced vertical and horizontal lines. After the target plane was aligned with the vertical laser light sheet, the test pipe was filled with the same water and Rhodamine solution used in the tests. An image was then captured by the camera and the pixel calibration calculated by measurements made with the image acquisition software and the knowledge of the actual grid spacing.

3.2. Cross section images of liquid film

A sequence of pairs of images of the cross section liquid film for a particular annular flow was captured and stored by the left and right cameras. Figure 4 aids in the explanation of image processing steps. Figure 4(a) presents the distorted original left and right images in reason of the angle of view. The stored images are dewarped by a calibration target, Fig. 5, using the Random Sample Consensus, RANSAC method, (Fischler & Bolles, 1981), as seen in Fig. 4(b). A global intensity histogram equalization is applied in the dewarped images, since the two images presented different grey level distributions due to differences in illumination. Then, this pair of images was joined to form a complete instantaneous image of the film cross section, Fig. 4(c). In order to assure a perfect matching of the left and right images, the position of the center of the calibration target as viewed by each camera was recorded during the calibration operation and is used to guide the join procedure. A circular black mask was applied to the inner surface of the pipe to trim ghost images resulting from film images out of the laser sheet and viewed by the cameras through the transparent tubes walls. Figure 4(d) presents the joined images with the overlaid mask. The images were binarized, Fig. 4(e), for measure the film thickness.

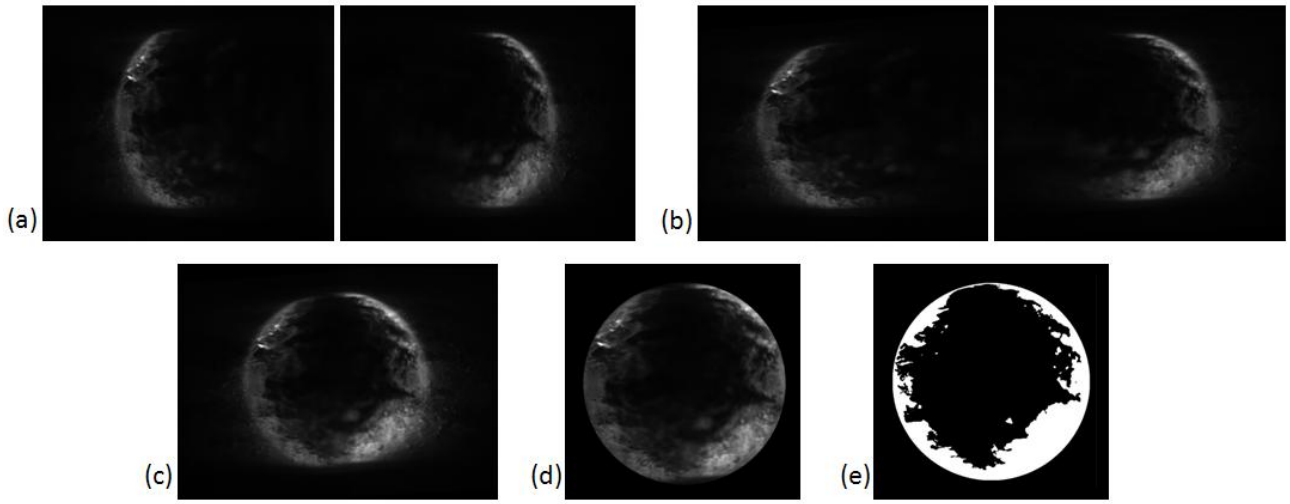

Figure 4. (a) Liquid film image as captured by the left and right cameras. (b) Dewarped left and right images. (c) Joined dewarped image. (d) Joined dewarped image with overlaid mask. (e) Binarized image.

Image distortion due to the side camera viewing was corrected by a specially written program that used images of a cylindrical target captured by the left and right cameras. The target, shown in Fig. 5, was introduced in the test tube through its exit section, in the same way as described before for the side view experiments. A grid of regularly-spaced dots was printed on the target face. As part of the calibration procedure, the target was inserted into the FEP test tube

and had its face aligned with the laser light sheet plane. The test tube was filled with the Rhodamine-water solution and one image of the target was captured with each camera and input to the dewarping routine developed.

The film amplitude measurement was performed for particular circumferential positions by counting along the radial direction the number of white pixels until the first black pixel (interface) is found, starting at the tube wall. The film thickness is corrected to take into account their circumferential location, due to the fact that image pixels are in the cartesian coordinate system. These circumferential positions are program inputs. It is interesting to mention that, different to the previous Farias (2010), the actual measurement procedure does not need to rotate the cross section image, saving computer time processing.

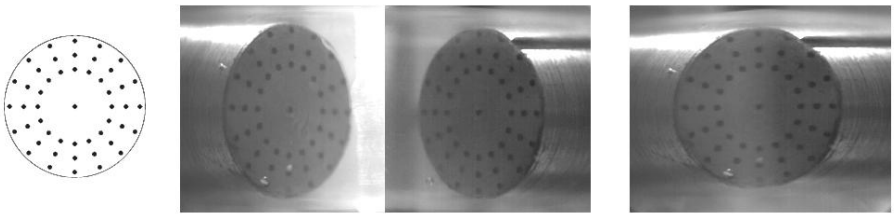

Figure 5. Calibration target, target as imaged by left and right cameras and after application of dewarping procedure and joining operation, respectively.

4. WAVE CHARACTERISTIC MEASUREMENTS

Quantitative information on the liquid film wave behavior was extracted from the thickness versus time data measured from the longitudinal and cross section time resolved images of the liquid film.

For the thickness versus time data, an acquisition frequency of 250 Hz was employed. Time-averaged liquid film thickness was obtained by averaging the thickness data over the record length. This value includes the contributions of large amplitude waves, as opposed to the data reported by Schubring and Shedd (2009) that only considers the base film thickness variation. Root-mean-square (RMS) values of the film thickness data were also calculated to aid in the flow characterization. Power spectra densities (PSD) of the film thickness time records were calculated employing 256 Hamming windows to filter the results (Harris, 1978) that would, otherwise, be too noisy due to the camera memory limitation.

The film thickness data obtained by the longitudinal camera viewing, gives a 512 x 512 pixel resolution which was sufficient to yield acceptable accuracy in the thickness measurements, since only the region ranging from the bottom wall to the pipe centerline was imaged by the camera. For this pixel resolution the camera memory allowed the record length of 13100 images, which at 250 Hz, translated to 52 s of recording time. However, in the case of the stereoscopic cross section data, each camera images half of the tube cross section, which requires the use of the 1024 x 1280 maximum pixel resolution offered by the camera in order to guarantee an acceptable accuracy in the measurements. With this pixel resolution, the camera memory allows capturing 6550 images, which correspond to a maximum recording time of 26 s at 250 Hz acquisition frequency.

To estimate the wave velocity, the time-record of the film thickness in two different axial positions in the image were selected and the cross-correlated (Bendat and Piersol, 1971). The wave velocity was obtained by dividing the axial distance between these two locations by the time corresponding to the cross-correlation peak. The distance between these two locations were chosen to minimize the uncertainty associated to the velocity. Preliminary tests conducted indicated that the camera acquisition frequency should be increased to 3000 Hz, translated to 4 seconds of the recording time, so that the cross correlation results provided acceptable accuracy for the wave velocity data. The statistical calculations just described were implemented using routines available in the Matlab® software.

5. RESULTS AND DISCUSSION

An experimental program was conducted with the objective of validating the optical technique developed. The experiments covered the ranges of water flow rates from 0.0052 to 0.0116 kg/s and air flow rates from 0.011 to 0.022 kg/s. These flow rates correspond to liquid superficial velocities of 0.056 to 0.112 m/s and air superficial velocities of 20 to 34 m/s. These operational conditions were chosen so as to allow comparison with results available in the literature. According to Taitel and Dukler (1976) flow map, these flow conditions are all within the annular flow regime region. All results to be presented were obtained with the 15-mm internal diameter pipe described in the experiments section, operating at atmospheric pressure level.

5.1 Space-time plots of longitudinal film thickness

Since the technique developed is based on the digital processing of time resolved images of the liquid film, high quality instantaneous images of longitudinal view of the liquid film were registered and available for analysis. An examination of these images provides valuable visualizations of the dynamics of the film.

A sequence of typical images illustrated in Fig. 6 is part of a set of 13100 images of the film captured at the bottom of the tube at 3000 frames per second for a superficial liquid velocity u_{sl}=*0.140 m/s* and a superficial gas velocity of u_{sg}=*20 m/s*. A continuous mark at the air-water interface overlaid on the cropped original images is seen in this figure.

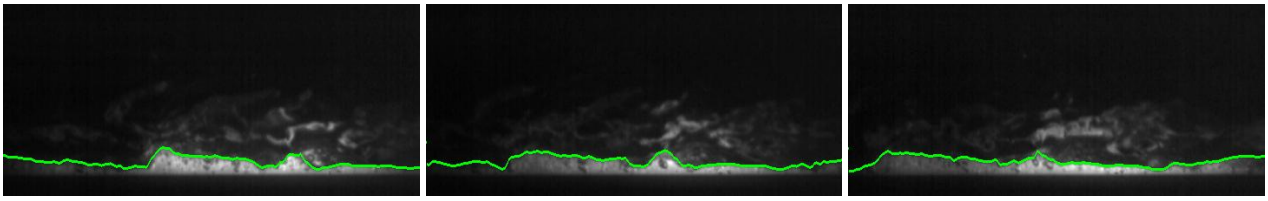

Figure 6. Measured liquid thickness film overlaid on original image for u_{sl}=*0.140 m/s* and u_{sg}=*20 m/s*.

The determination of the complete air-water interface in each image frame captured allows the construction of space-time maps displaying in details the evolution and interaction of the waves present in the liquid film. Figure 7 presents examples of such space-time maps for a superficial liquid velocity of u_{sl}=*0.140 m/s* and a superficial gas velocity of u_{sg}=*20 m/s*. The maps were formed by a sequence of longitudinal cross sections views of the liquid film at the bottom of the tube captured during a 0.05 s interval. The width of the images in the flow domain was approximately equal to 25 mm. In these figures, *x* is the longitudinal direction along the pipe length, *t* is the time and *h* is the film thickness. These maps are displayed in an isometric 3D view and a corresponding top view. Similar space-time flow maps were presented in the work of Alekseenko *et al.* (2008), where an intensity-based LIF technique was implemented using a linear-array high frame rate camera. An observation of these maps shows interesting features of the wave dynamics. In these figures, the wave propagation velocities are equal to the slope of the film thickness isovalues. In Fig. 7(a) the higher amplitude waves are seen to travel faster than the smaller amplitude waves. Further, a disturbance wave can be shown in Fig. 7(b).

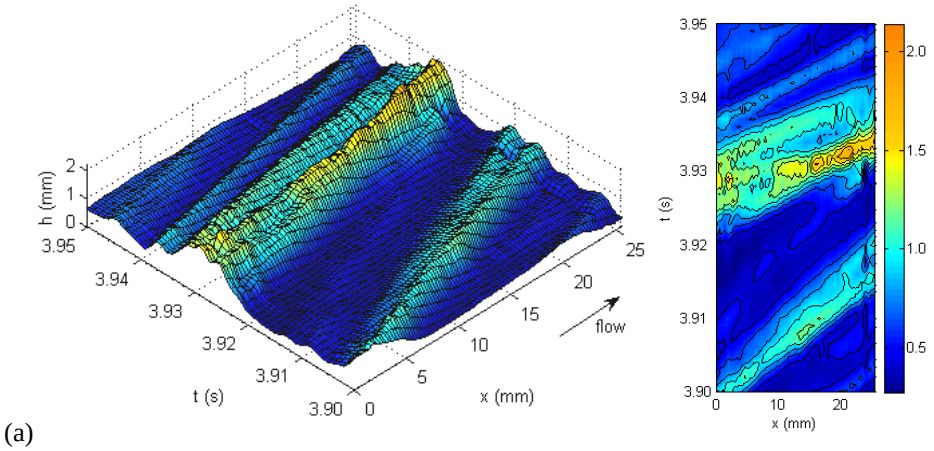

(a)

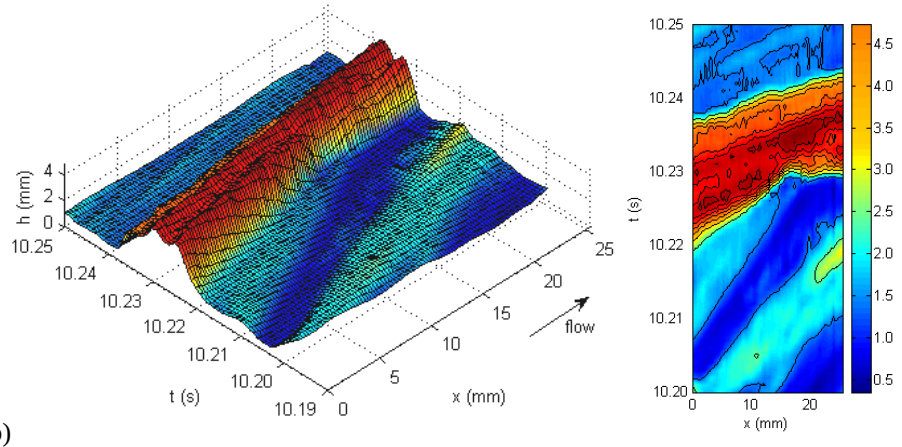

(b)

Figure 7. Space-time maps showing the evolution of the waves in the liquid film for u_{sl}=*0.140 m/s* and u_{sg}=*20 m/s*.

5.4 Time-averaged and RMS film thickness

Average film thicknesses at the bottom of the pipe obtained from the measured time records for all operating conditions investigated are presented in Fig. 8(a). The results indicate that the average liquid film at the bottom of the tube is a decreasing function of the superficial gas velocity, depending weakly on the superficial liquid velocity for the range of flow rates investigated. These trends agree with previous results available in the literature (Jayanti *et al.*, 1990 and Paras and Karabelas, 1991). Root mean square values (RMS) of the film thickness at the bottom of the tube can also be extracted from the time-resolved thickness data obtained for a axial position of the image predetermined. In Fig. 8(b) the ratio of the RMS thickness data to the time-averaged thickness (h_{RMS}/h) is plotted as a function of the superficial gas velocity, for different values of the superficial liquid velocity. This ratio is a measure of the intensity of the film thickness fluctuation, and reaches a peak of 67% for the conditions corresponding to the lowest gas velocity (20 m/s) and intermediate liquid superficial velocity (0.084 m/s). These results are in agreement with the work of Paras and Karabelas (1991) that employed resistive probes.

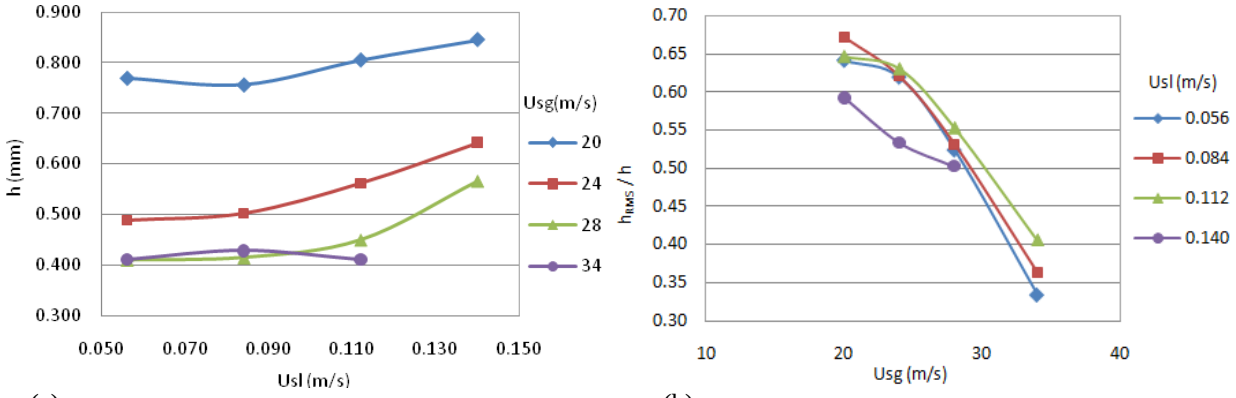

(a) (b)

Figure 8. (a) Time-averaged liquid film thickness at the bottom of the tube. (b) Ratio of the RMS liquid film thickness to the time-averaged thickness.

The measured time-varying liquid film thickness data can be used to construct histograms displaying the probability of occurrence of the different peaks in film thickness, called wave amplitudes. In order to allow for an assessment of the effects of the gas and liquid flow rates on the film thickness distribution and to avoid overcrowding the figure, histograms for different flow operational conditions were plotted in the same diagram as continuous lines in Fig. 9(a).

The effect of the superficial gas velocity on the film thickness distribution is clearly seen in Fig. 9(a) where the thicknesses histograms are plotted for liquid superficial velocity equal to 0.112 m/s and for different values of the gas superficial velocity. An inspection of Fig. 9(a) reveals that the thickness distribution changes significantly as the gas velocity is increased from 20 to 34 m/s. Indeed, it can be verified that the thickness distribution changes markedly from 20 to 24 m/s, a gas superficial velocity beyond which the majority of the thickness values are tightly grouped around the 0.5-mm bin, which is an indication of the regularization effect that the gas imposes on the wave character of the liquid film.

5.5 Wave velocity results

Figure 9(b) presents the wave velocity values obtained for all the experiments conducted. In this figure, measured wave velocities are plotted as a function of the superficial gas and liquid velocities. Not only was the correct dependence of the wave speed with liquid and gas superficial velocities captured by the optical technique developed, but also the numerical values obtained are in good agreement with the results from Schubring and Shedd (2008) and Fukano and Ousaka (1989).

5.6. Power spectra density of thickness time records

Figures 10(a) and (b) present power spectra density (PSD) plots of the time-resolved thickness data for the flow conditions indicated. These PSD results were selected among all the flow conditions tested as an example to convey the capability of the optical technique implemented to extract spectral information from the film thickness data. The presentation of Fig. 10 shows the influence of the gas velocity on the PSD of the film thickness time data for two values of the liquid superficial velocity, namely, 0.084 and 0.112 m/s. The influence of the gas superficial velocity is significant for both liquid flow values. A clear increase in the dominant frequency with the superficial gas velocity is observed for both superficial liquid velocities, a trend also reported in the literature (Jayanti *et al.*, 1990 and Paras and Karabelas, 1991).

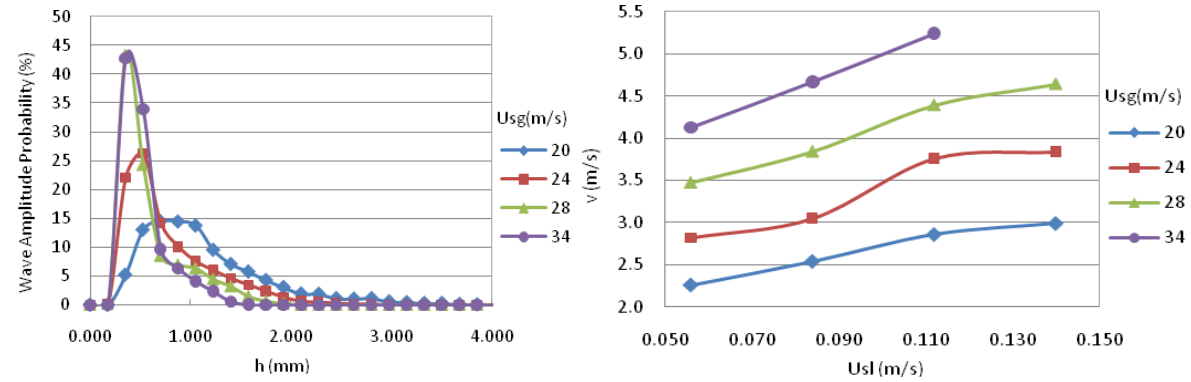

(a) (b)

Figure 9. (a) Histogram of liquid film thickness for u_{sl}=*0.112 m/s* and different gas superficial velocities. (b) Wave velocity measured at the bottom of the tube for u_{sg}=34 m/s and u_{sl}=0.112 m/s

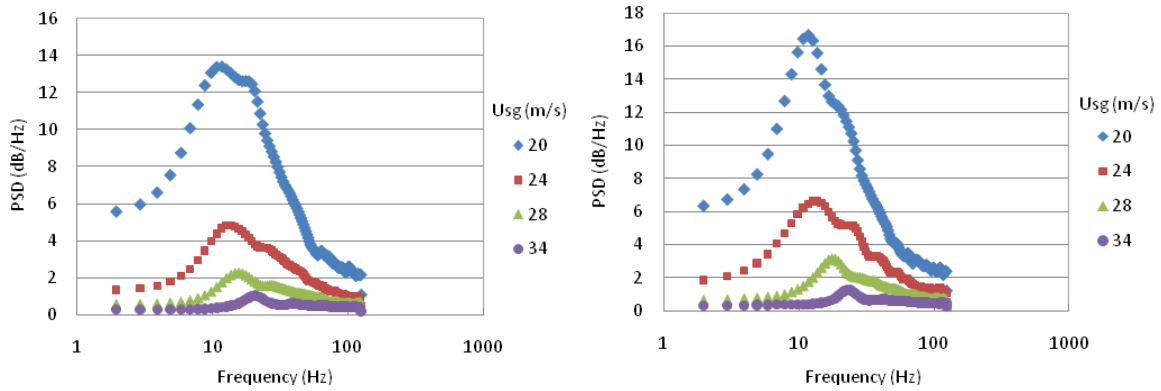

(a) (b)

Figure 10. PSD of film thickness time variation for different gas superficial velocities for (a) u_{sl} =0.084 m/s and (b) u_{sl} =0.112 m/s.

5.7 Space-time plots of cross-sectional film thickness

High quality instantaneous images of cross-sectional view of the liquid film were registered at 2000 frames per second and are available for analysis of the dynamics of the film. These images carry quantitative information on the film statistical and spectral properties around the tube perimeter. By applying the image processing procedures presented in the present paper, measurements of film thickness information on the liquid film can be determined for the complete cross section of the liquid film. Figure 11 presents a sequence of cross section images captured, where the film thickness was measured by the technique developed at every 5 degrees around the tube circumference, as indicated by the marks overlaid on the joined dewarped image, under the conditions of superficial air and liquid velocities of, respectively, 20 m/s and 0.140 m/s. Visual analysis of a slow motion sequence of the images allows the observation of the circumferential motion of the liquid film climbing and descending the tube wall.

Farias et al. (2010) attested the potential of the cross-sectional measuring technique with a comparison of the film thickness and wave frequency of the longitudinal measurements with those obtained by the cross section measurements.

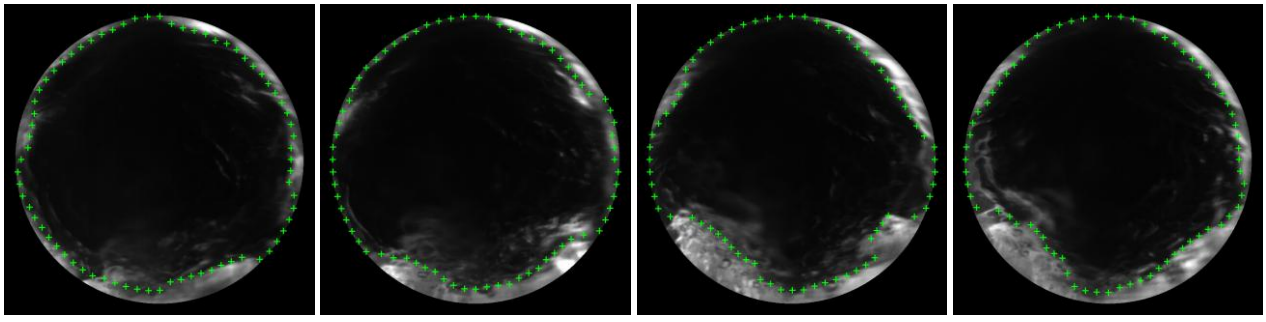

Figure 11. Measurement of instantaneous film thickness around the tube circumference for u_{sg} = *20 m/s* and u_{sl} = *0.140m/s*.

The determination of the air-water interface around the tube circumference for a particular axial position of the tube in each image frame captured allows the construction of space-time maps displaying in details the evolution and interaction of the waves. Figure 12 presents examples of such space-time maps for u_{sl}=*0.140 m/s* and u_{sg}=*20 m/s*. In the figure, *angle* is the circumferential position, *h* is the film thickness and *t* is the time. The circumferential position is measured in the counterclockwise direction, starting at the bottom. The time signal of the film thickness can be measured at many circumferential positions (in this case at 72 positions, every 5 degrees) giving us a spatial reconstruction of the film in the annular flow. The maps were formed by a sequence of cross sections views, as shown in Fig. 11, of the liquid film captured during a 0.1 s interval. Similar results were presented in the work of Belt et al. (2007) using a conductivity-based technique for vertical annular flow.

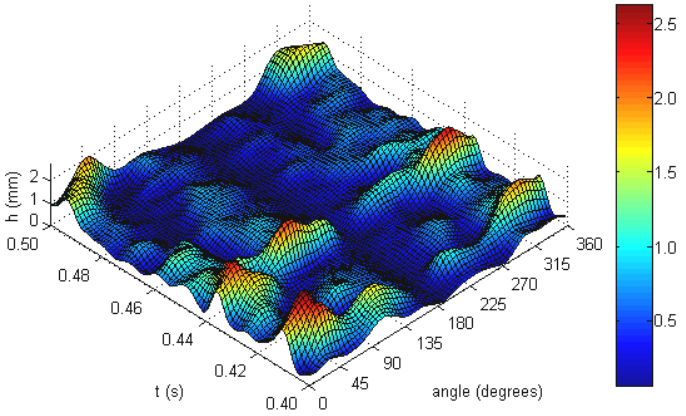

Figure 12. Space-time map showing the evolution of the waves in the liquid film for u_{sl}=*0.140 m/s* and u_{sg}=*20 m/s*.

Figure 12 shows problems in the liquid film thickness measurement near angles of 0, 90, 180 and 270 degrees. The highest thickness liquid film does not occur at the bottom of the tube, as is expected, and valleys in 90, 180 and 270 degrees positions appear. These problems happened probably due to illumination. The fluorescent light emitted by the liquid film of the tube is attenuated as the light travels inside the gas-phase core. This problem is more evident at the bottom (0 degrees) and at the top (180 degrees) of the tube in the space-time map. As can be observed in Fig. 4(a), only the side view of each camera is visualized for the same reason. Furthermore, at 90 and 270 degrees positions the detection of the film thickness was not efficient. In these positions a poor illumination occurs due to a decreasing of the intensity of the laser sheet. The ongoing work is trying to overcome these problems.

6. CONCLUDING REMARKS

The present paper exposed an optical technique developed for measuring the statistical and spectral properties of time-varying liquid film thicknesses in horizontal, air-water annular pipe flow. The technique proposed builds on existing visualization techniques described in the literature. It uses tube material with index of refraction that nearly matches that of water in order to permit the visualization of thin liquid films adjacent to the tube wall. Laser induced fluorescence was employed to separate the intense light reflected from the air-water interfaces and allow the recording of the desired liquid film images. Recording of the images was conducted with high frame rate cameras what produced time-resolved data with good spatial resolution. The quality of the film images obtained allowed the visualization of the wave behaviour of the liquid film.

Two versions of the optical technique were implemented. In one technique, a longitudinal section of the film defined by a pulsed laser light sheet is imaged with a high frame rate camera synchronized with laser firing. The second technique employed two high frame rate cameras in a stereoscopic setup to yield an instantaneous view of the complete cross section of the liquid film.

Specially developed image processing routines were applied to improve image contrast, to calibrate the images, and to correct for the distorted views associated with the stereoscopic setup. Quantitative information on the statistical properties of the liquid film was extracted from the digital images for both, the longitudinal and stereoscopic setups. The processed results included time-resolved film thickness values, time-averaged and RMS thickness values, wave velocities and power spectra density of the thickness data. Space-time maps were also obtained providing valuable information on the wave interaction process. The influence of superficial gas and liquid velocities on these quantities was identified and compared with data available in the literature obtained by different measuring techniques. Good agreement was obtained with the data from the literature, which served to validate the technique. Histograms of the film thickness distribution were also presented to complement the statistical characterization of the liquid film time varying data.

Overall, the technique presented good results and can potentially contribute to a better understanding of annular liquid-gas two-phase flows.

7. ACKNOWLEDGEMENTS

The authors gratefully acknowledge the support awarded to this research by Petrobras R&D Center. Our gratitude is also extended to the Brazilian Research Council, CNPq, for the scholarships and continued support to our research activities. The authors also thank the enthusiastic cooperation from undergraduate students Bruno Dreux and Carlos Eduardo Correia.

8. REFERENCES

Alekseenko SV, Antipin VA, Cherdantsev AV, Kharlamov SM and Markovich DM (2008). Investigation of waves interaction in annular gas-liquid flow using high-speed fluorescent visualization technique. Microgravity Sci. Technol. 20:271-275.

Belt RJ, Van't Westende JMC, Prasser HM and Portela LM (2010). Time and spatially resolved measurements of interfacial waves in vertical annular flow. Int. J. Multiphase Flow 36:570-587.

Bendat JS and Piersol AG (1971). Random data: Analysis and measurement procedures. Wiley-Interscience, New York.

Butterworth D and Pulling DJ (1972). A visual study of mechanisms in horizontal annular air-water flow. Atomic Energy Research Establishment, M-2556, Berkshire.

Farias PSC (2010). Optical liquid film characterization in two-phase, annular, horizontal flow. Master Dissertation, PUC-Rio (in Portuguese).

Fischler MA and Bolles RC (1981). Random Sample Consensus: A Paradigm for Model Fitting with Applications to Image Analysis and Automated Cartography. Communications of the ACM 24: 381–395.

Fukano T and Ousaka A (1989). Prediction of the circumferential distribution of film thickness in horizontal and near-horizontal gas-liquid annular flows. Int. J. Multiphase Flow. 15:403-419.

Harris FJ (1978). On the use of windows for harmonic analysis with the discrete Fourier transform. Proc. IEEE, 66: 172-204.

Hewitt GF, Jayanti S and Hope CB (1990). Structure of thin liquid films in gas-liquid horizontal flow. Int. J. Multiphase Flow, 16:951-957.

Jayanti S, Hewitt GF and White SP (1990). Time-dependent behaviour of the liquid film in horizontal annular flow. Int. J. Multiphase Flow 16:1097-1116.

Koplin CR (2004). Local liquid velocity measurements in horizontal, annular two-phase flow. PhD Thesis. University of Wisconsin-Madison.

Oliveira GH and Portela LM (2010). The interfacial shear-stress as a film pumping mechanism in annular pipe-flow. 7th Int. Conf. Multiphase Flow, Tampa USA.

Paras SV and Karabelas AJ (1991). Properties of the liquid layer in horizontal annular flow. Int. J. Multiphase Flow 17: 439-454.

Raffel M, Willert CE, Wereley ST and Kompenhans J (2007). Particle image velocimetry – A practical guide. 2nd ed. Springer, Berlin, Heidelberg, New York.

Rodríguez DJ and Shedd TA (2004). Cross-sectional imaging of the film in horizontal two-phase annular flow. ASME Heat Transfer/Fluids Eng. Summer Conf., Charlotte, USA, HT-FED04-564452004.

Schubring D and Shedd TA (2009). Critical friction factor modeling of horizontal annular base film thickness. Int. J. Multiphase Flow 35:389-397.

Schubring D and Shedd TA (2008). Wave behavior in horizontal annular air-water flow. Int. J. Multiphase Flow 34:636-646.

Shedd TA and Newell TA (1998). Automated optical liquid film thickness measurement method. Review of Scientific Instruments 69:4205-4213.

Sutharshan B, Kawaji M and Ousaka A (1995). Measurement of circumferential and axial liquid film velocities in horizontal annular flow. Int. J. Multiphase Flow 21:193-206.

Taitel Y and Dukler AE (1976). A model for predicting flow regime transitions in horizontal and near horizontal gas–liquid flow. AIChE Journal 22:47-55.

Taylor NSH and Nedderman RM (1968). The coalescence of disturbance waves in annular two phase flow. Chem. Eng. Science 23:551-564.

Vassalo P (1999). Near wall structure in vertical air-water annular flows. Int. J. Multiphase Flow 25:459-476.